Acta Biotheoretica (2026) 74:5
https://doi.org/10.1007/s10441-025-09514-3

REGULAR ARTICLE

Quantifying Uncertainty and Sensitivity in an Alzheimer's Disease Model: A Mathematical Approach

Mitali Maji[1] · Laurent Pujo-Menjouet[2] · Subhas Khajanchi[1]

Received: 11 April 2025 / Accepted: 19 December 2025

Abstract

To understand the dynamics of Alzheimer's disease, we formulate a generalized mathematical model based on three events: aggregation of disease-related proteins, activation of immune cells and initiation of inflammation. We incorporate functional forms in the model to represent the complex biological interactions between components related to Alzheimer's disease. We take explicit forms depending on the properties of functions in the model. We describe the system dynamics by locating biologically feasible steady states, determining stability properties and identifying the effective parameters. Parameters are estimated using two methods: biological literature and data fitting. We perform sensitivity and uncertainty analyses to identify the most influential parameters. Partial Rank Correlation Coefficient and scatter plots are used to visualize global sensitivity. Our results reveal that lower activation rate and higher proliferation rate of microglia may contribute to a reduction in toxic protein aggregate levels, thus slowing the disease's early progression.

Keywords Neuroinflammation · Amyloid beta oligomers · Tau protein · NFTs · Microglia

✉ Subhas Khajanchi
subhas.maths@presiuniv.ac.in

Mitali Maji
mitali.rs@presiuniv.ac.in

Laurent Pujo-Menjouet
pujo@math.univ-lyon1.fr

[1] Department of Mathematics, Presidency University, 86/1 College Street, Kolkata 700073, India

[2] Universite Claude Bernard Lyon 1, CNRS, Centrale Lyon, INSA Lyon, Université Jean Monnet, ICJ UMR5208, Inria, 69622 Villeurbanne, France

Published online: 03 January 2026

1 Introduction

One of the most prevalent forms of dementia is Alzheimer's disease (AD), which is a progressive neurological disorder that affects memory, thinking, personality and behavior. Approximately 55 million people worldwide are affected by the disease currently and the number of cases continues to rise due to a lack of effective cures and preventive measures. Mostly, AD ranks as the seventh leading causes of death globally (World Health Organization 2024).

AD is triggered by the abnormal accumulation of, on one hand, amyloid beta (Aβ) protein in the brain, forming extracellular Aβ plaques, and on the other hand, tau (τ) proteins aggregating intracellularly into neurofibrillary tangles (NFTs). This affects neuronal functioning and connectivity, leading to progressive loss of brain function and the affected brain areas include the hippocampus and cerebral cortex.

AD is a multifactorial condition and the application of mathematical models represents just one facet of its comprehensive study. Developing mathematical models can greatly enhance our understanding of the fundamental causes of AD. Numerous mathematical models have already been investigated to understand disease progression and many studies are currently ongoing. The work by Hao and Friedman (2016) presents a mathematical model of AD involving the key elements, including neurons, astrocytes, microglia, macrophages, cytokines, Aβ aggregation and τ protein dynamics. The model simulates the effects of various drugs and suggests that combined therapy with tumor necrosis factor-α (TNF-α) inhibitors and anti-Aβ drugs could be more effective in slowing disease progression. Chamberland et al. (2024) extended the model of Hao and Friedman (2016) into a more comprehensive and biologically grounded framework by incorporating key factors such as the APOE gene and diabetes-related mechanisms (insulin and glycogen synthase kinase-3 (GSK-3)). The study of Bertsch et al. (2023) introduces a graph mathematical framework that captures the interplay of Aβ diffusion in the extracellular space and τ propagation along neuronal connectivity. In neurodegenerative diseases, protein-protein interactions play a critical role. Nonlocal continuous and network models have been suggested due to the importance of concentration variations in Aβ and τ proteins in the onset and development of AD (Pal and Melnik 2022; Thompson et al. 2020). A temporal mathematical model involving the key components for AD-like microglia, astrocytes, neurons and Aβ was given by Puri and Li in their work (2010). In the study of Craft et al. (2002), authors designed a mathematical compartmental model to explain the accumulation of the Aβ protein within the brain, cerebrospinal fluid (CSF) and plasma. To get a deeper understanding of the dynamics of oligomer formation and its connection to the onset of AD, Lindstrom et al. (2021) created a mathematical model of the oligomerization process. Ciuperca et al. (2024) developed a novel mathematical model for the development of AD, taking into account the interactions between Aβ monomers, oligomers, plaque, microglia and interleukins. A series of work has been done on AD with different types of mathematical approaches that are reflected in the review article by Maji and Khajanchi (2025).

This work focuses on a mathematical model that involves the complex interactions between disease-related proteins and glial cell. Since the parameter values for the model will be obtained from various sources, sensitivity analysis (SA) and uncer-

tainty analysis (UA) have been conducted to find most sensitive parameters. SA and UA are two important methods to understand the correlation between the model's output and input. To enhance this understanding, we apply SA and UA to our complex model. UA and SA both are related to each other but they are not identical. UA generally examines the variability or variations of model output in the presence of a known distribution in input parameters. Hence, this uncertainty in the inputs limits in getting a specific conclusion to the model's output. These imperfections are measured with UA and it treats the simulation result as probabilistic rather than deterministic (DesignBuilder Software Ltd 2024). One of the most well-known techniques to do this UA is Monte Carlo (MC) simulation which is a sample-based method. There are several sampling techniques to extract parameters from probabilistic distributions, including Simple MC sampling, Latin hypercube sampling (LHS) and Importance sampling. In this work, we use the LHS method in our simulation. The LHS method, a stratified sampling approach within MC framework, was first introduced by McKay in 1979 (McKay et al. 2000). On the other hand, SA is a method that determines how changes in the input affect the output and identifies which input uncertainties have the most significant impact. SA involves performing multiple simulations by varying the input around a small value. Global SA assesses the impact of varying all input parameters simultaneously over their entire range of values Tian (2013); Hamby (1995). Global SA techniques are commonly implemented using MC simulations (sampling-based methods). A useful initial approach when applying sampling-based methods is to utilize scatter plots.

Although some models, such as those by Hao and Friedman (2016); Chamberland et al. (2024) and Bertsch et al. (2023) considered both Aβ and τ, they did so within either complex multi-scale systems or graph-based spatial frameworks. Here, we present a minimal and biologically motivated model that explicitly incorporates Aβ oligomer and NFTs formation, τ phosphorylation and microglial dual nature (protective and harmful), thereby capturing pathological feedback loops and the bi-directional link between inflammation and Aβ production. Hence, the main objective of this study is to introduce and investigate a biological-based mathematical model for AD, which involves the most important disease-related proteins and immune responses. Next, we improve the model's predictive power by fitting the data to specific model components, which allows us to have more precise simulations, and to better understand the disease's progression and potential treatment outcomes.

The paper is organized as follows. Section 2 presents the formulation of the mathematical model through a system of differential equations where the interactions and processes are described by specific functional relations. We provide some basic properties of the model. We determine the steady states and do the stability analysis in Sect. 3. Based on the properties of functions in the model, we put the explicit forms to the functions in Sect. 4. Section 5 covers the numerical simulation of the analytical results, along with parameter estimation, SA and UA. Finally, a brief discussion and conclusion are provided in Sect. 6.

2 The Model

2.1 Biological Background

AD is a complex disease with multiple contributing factors. This disease can be characterized by the accumulation of protein, activation of glial cells, production of inflammation or oxidative stress, brain damage, neuronal loss, etc. Al-Ghraiybah et al. (2022); Tonnies and Trushina (2017). Here, we mainly focus on three important factors involved in AD: Aβ protein, τ protein and a glial cell. The following portion provide details descriptions of the contributions, background and interconnections of proteins, microglia and inflammation.

- **Aβ protein:** Aβ protein is a small peptide derived from the larger amyloid precursor protein (APP). The Aβ protein is typically composed of 36 to 43 amino acids. Aβ42 is a specific form of the Aβ peptide, consisting of 42 amino acids. Aβ42 is considered particularly neurotoxic as it has high tendency to aggregate more readily than other forms like Aβ40 (Sandberg et al. 2022). It can form soluble oligomers that contribute to the formation of Aβ plaques observed in AD (Song et al. 2022; Maji and Khajanchi 2024). Aβ oligomers are small, soluble aggregates of Aβ peptides, while Aβ plaques are large, insoluble aggregates of Aβ peptides that form in the extracellular spaces of the brain (Chen et al. 2017). Aβ oligomers are considered the most toxic form of Aβ (Goure et al. 2014). Numerous studies (Craft et al. 2002; Chen et al. 2019) show that Aβ aggregation and its processes strongly impact AD. Aβ proteins and their polymer units, which include Aβ monomers, dimers, polymers, oligomers, fibrils and plaques, are considered contributing factors in the progression of AD. It is believed that Aβ plaques are toxic to the brain and are among the primary factors responsible for the advancement of the disease. But recent studies show that the Aβ oligomers are more toxic to the brain than plaques (Huang and Liu 2020). Hence, we give importance to the Aβ monomer and oligomers in this work.
- **τ protein:** τ protein is also critical to the pathogenesis of AD. τ is a microtubule-associated protein that helps neurons to maintain their internal structure. When τ undergoes aberrant chemical changes, this causes τ proteins to separate from microtubules and form insoluble tangles inside neurons, known as neurofibrillary tangles (NFTs). τ protein hyperphosphorylation is an important phase in the development of AD that is strongly related to the influence of Aβ oligomers (De Felice et al. 2008). Indeed, these oligomers interact with neuron surface receptors and activate intracellular signaling cascades and kinases such as GSK-3β and cyclin-dependent kinase-5 (CDK-5) (Zhang et al. 2021; Rankin et al. 2007). These kinases phosphorylate τ proteins. As a result, hyperphosphorylated τ clumps into insoluble fibrils that form NFTs.
- **Microglia and inflammation:** Rather than proteins, neuron-supporting cells, called glial cells, contribute significantly to disease progression through their roles in neuroinflammation and immune response. Several types of glial cells, including astrocytes, microglia and oligodendrocytes are implicated in the disease progression. Microglia are the most prevalent immune cells in the brain

(Morimoto and Nakajima 2019). Cytokines are signaling proteins released by microglia. Finally, microglia and neuroinflammation hold a significant place in the pathology of AD. There is still a question about the protectiveness and harmfulness of microglia. In AD, microglia have a dual role in disease progression, as they are crucial for clearing Aβ deposits but also contribute by releasing cytotoxic mediators (Doens and Fernandez 2014). The presence of Aβ accumulation and NFTs triggers the activation of microglia (Salvadores et al. 2022; Ohm et al. 2021). In the early stage of AD, activated microglia behave like neuroprotective and remove harmful aggregates using a process known as phagocytosis (Zhang et al. 2021). This early reaction protects the brain by removing toxic Aβ. However, microglia do not efficiently clear Aβ, as a result, Aβ protein again starts accumulating leading to prolonged activation of these immune cells. This long-term activation causes microglia to become pro-inflammatory, releasing cytokines such interleukin-1β (IL-1β), TNF-α and interleukin-6 (IL-6) (Zhang et al. 2021; Magni et al. 2012). These cytokines contribute to neuroinflammation, which may cause neuronal and synaptic damage, and also accelerate cognitive decline. On the other hand, these pro-inflammatory cytokines play a crucial role in AD by promoting the aggregation of Aβ monomers. Neuroinflammatory cytokines can increase amyloid precursor protein (APP) levels and unregulate the activity of β -secretase and γ-secretase (Meraz-Rios et al. 2013). This leads to an increase of the production of Aβ monomer (Alasmari et al. 2018).

2.2 Model Development

The development of our model begins by identifying the key biological components related to AD, including Aβ, τ protein and immune responses such as microglial activation and cytokine production, degradation and interaction dynamics of these proteins as well as the role of neuroinflammation in disease progression. We include below the underlying mechanism into the mathematical model:

- Aβ proteins simulate their own production, aggregation and clearance, eventually forming Aβ oligomers,
- τ proteins misfold and potentially interact with Aβ proteins,
- misfolding of τ proteins results in formation of NFTs,
- microglial activation is modeled as part of the immune response, where activated microglia influence the clearance of Aβ and produce cytokines,
- microglia show both protective and neurotoxic role reflecting its complex behavior in AD progression, regardless the stages of AD progression,
- production and release of cytokines occur by activated microglia, which influence the inflammatory environment,
- cytokines help in the production of Aβ monomer.

The above underlying mechanism in AD are schematically represented through a diagram given in Fig. 1.

Based on these events, we formulate a system of differential equations to describe the interactions between these proteins and the immune system.

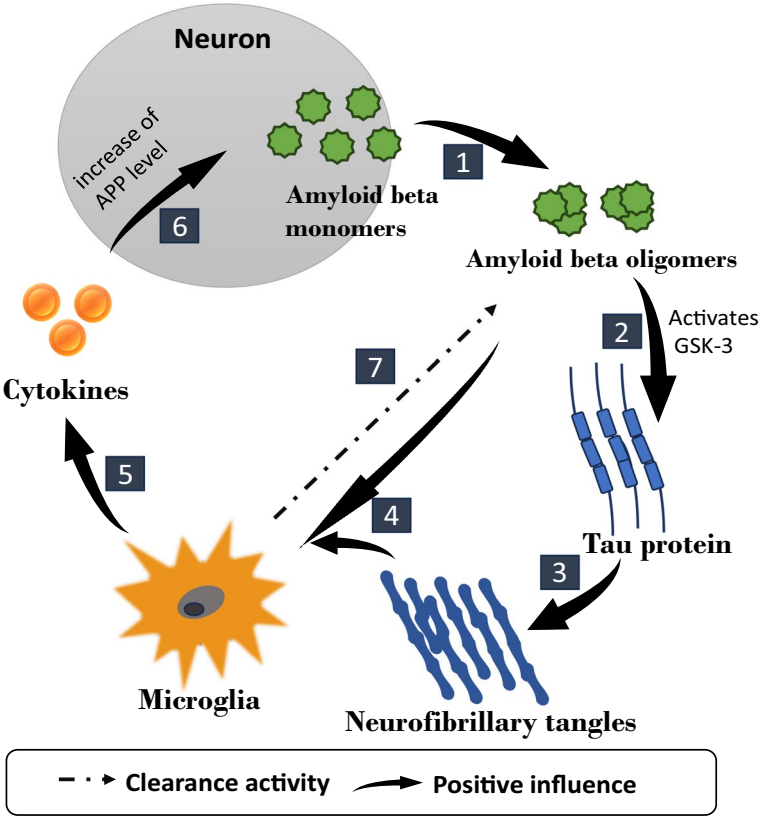

Fig. 1 A schematic diagram for the progression of AD to reflect the model (1) that involves the following components: Aβ monomers, Aβ oligomers, τ protein, NFTs, microglia and cytokines. Explanation of the schematic diagram: 1. Aβ oligomers are aggregated from Aβ monomers, 2. τ proteins are phosphorylated by Aβ oligomers through activation of GSK-3, 3. The phosphorated τ proteins accumulate and form NFTs, 4. Microglia are activated by Aβ oligomers and NFTs, 5. Activated microglia produce cytokines, 6. Aβ monomers are produced by cytokines through increasing APP levels, neuronal stress due to Aβ oligomers is not explicitly considered, 7. Aβ oligomers are cleared from the brain by early-stage activated microglia

2.3 Model Formulation

A system of six ordinary differential equations is employed to describe our proposed dynamics of AD. The considered model populations at time $t \geq 0$ are given by:

- $A_m(t)$ denotes the concentration of Aβ monomers;
- $A_\beta(t)$ represents the concentration of Aβ oligomers;
- $\tau_p(t)$ corresponds to the concentration of τ proteins;
- $N_F(t)$ signifies the concentration of NFTs;
- $M(t)$ indicates the density of microglia;
- $I(t)$ refers to the concentration of cytokines.

The mathematical model reads as

$$\begin{cases} \dfrac{dA_m}{dt} = A_m r(A_m) + A_m f(I) - h(A_m), \\ \dfrac{dA_\beta}{dt} = h(A_m) - s(M)A_\beta - \delta_\beta A_\beta, \\ \dfrac{d\tau_p}{dt} = \gamma_p A_\beta - \delta_p \tau_p - g(\tau_p), \\ \dfrac{dN_F}{dt} = g(\tau_p) - \delta_N N_F, \\ \dfrac{dM}{dt} = \gamma_M - \delta_M M + (f_M(A_\beta) + g_M(N_F))(\tilde{M} - M)M, \\ \dfrac{dI}{dt} = h_I(A_\beta)M - \delta_I I, \end{cases} \tag{1}$$

with the initial conditions $A_m(0) \geq 0, A_\beta(0) \geq 0, \tau_p(0) \geq 0, N_F(0) \geq 0, M(0) \geq 0$ and $I(0) \geq 0$. The descriptions of parameters and functions in the above model (1) are given below:

- $r(A_m)$ is the growth term of Aβ monomer;
- *f*(*I*) describes the production activation of Aβ monomer by cytokines;
- $h(A_m)$ represents the formation of Aβ oligomers from Aβ monomers;
- *s*(*M*) is the clearance rate of Aβ oligomers by activated microglia;
- γ_p denotes the phosphorylation of τ protein by Aβ oligomers;
- $g(\tau_p)$ signifies the formation of NFTs from τ proteins;
- γ_M is the production rate of microglia;
- $f_M(A_\beta)$ and $g_M(N_F)$ denote the activation of microglia by Aβ oligomers and NFTs, respectively. We introduce $\tilde{M}$ as the local carrying capacity representing the maximum number of microglia that can be present around a neuron. With this, it is considered that surrounding the neuron, the number of activated microglia cannot exceed a certain threshold $\tilde{M}$;
- $h_I(A_\beta)$ describes the production of cytokines that depends on the concentration A_β;
- δ_β, δ_p, δ_N, δ_M and δ_I are the degeneration rates of Aβ oligomers, τ protein, NFTs, microglia and cytokines, respectively.

2.4 Model Assumptions

To investigate the dynamics of system (1), we consider the subsequent biologically takeable assumptions delineating the characteristics of the functions mentioned in the system (1). All the functions *r*, *f*, *h*, *s*, *g*, f_M, g_M and h_I are supposed continuously differentiable functions.

- **Properties of the growth rate** $r(A_m)$**:** $r(A_m)$ needs to satisfy $r(0) = r_m > 0$ and $r(k_m) = 0$, where $k_m > 0$ is the carrying capacity of Aβ monomers in absence of any inflammation. Also, it is decreasing on [0, k_m].

- **Properties of $f(I)$:** inflammation plays an important role in the activation of Aβ monomer production. We consider the function f in such a way that if the population of cytokines becomes too large, the production of Aβ monomer cannot exceed infinity; f is increasing, $f(0) = 0$ and $\lim_{I\to\infty} f(I) = \mu_I > 0$.
- **Properties of $h(A_m)$:** the expression $h(A_m)$ denotes the process of oligomerization, where monomers combine to form oligomers. In other words, the formation of oligomers needs at least two monomers to come together. Hence, we consider that h is increasing and $h(0) = 0$. Moreover, $\lim_{A_m\to\infty} h(A_m) = +\infty$. We can even determine the exact form of $h(A_m)$ by the monomer-oligomers reaction process. Let us assume, as in Dear et al. (2024); Maji and Khajanchi (2024); Portet and Arino (2008); Dear et al. (2020), that oligomers are produced by the following $n-1$ reactions from monomers in such a way that

$$R_i + A_m \rightleftharpoons R_{i+1}, \tag{2}$$

for $i = 1, 2, ..., (n-1)$. R_i represents the aggregates of i-monomers for $i = 2, ..., n$, where $n \in \mathbb{N}$, and the reaction rate of each equation is given by r_i. By taking all the equations at the equilibrium, we get $R_2 = r_2 A_m^2$, $R_3 = r_3 R_2 A_m = r_3 r_2 A_m^3$, and so on with $R_n = \mu_m A_m^n$, where μ_m is the formation rate of oligomers and it is given by $\mu_m = r_1 r_2 ... r_n > 0$. We set $h(A_m) = \mu_m A_m^n$ with $n > 1$.

- **Properties of $s(M)$:** microglia increases the clearance efficiency of Aβ oligomers up to some saturation limit, that is, s is an increasing function, followed by $s(0) = 0$, $\lim_{M\to\infty} s(M) = \tilde{\mu}(> 0)$, a constant, and s' is decreasing.
- **Properties of $g(\tau_p)$:** the phosphorylated τ proteins assemble into protofibrils, called paired helical filaments (PHFs), and then into NFTs. Using a similar concept (Townsend et al. 2020; Chen et al. 2024) to model the formation of protein monomers into oligomers, protofibrils, and fibrils (e.g., Aβ protein), we define the aggregation term as $g(\tau_p) = \mu_p \tau_p^m$, where $m > 1$ represents the number of τ_p monomers required to form fibrils and μ_p is the formation rate of fibrils.
- **Properties of $f_M(A_\beta)$:** as the concentration of Aβ oligomers increases, it implies more activation of microglia. We take f_M in such a way that, it is increasing and $f_M(0) = 0$. We assume that the microglial response can accelerate or remain constant with increasing Aβ oligomers with no saturation limit. Hence, f_M' is nondecreasing.
- **Properties of $g_M(N_F)$:** since NFTs are implicated in inflammation and immune response, more NFTs lead to greater microglial activation. g_M is an increasing function with $g_M(0) = 0$. Here also we assume no biological limits to the activation of microglia is considered and g_M' is nondecreasing.
- **Properties of $h_I(A_\beta)$:** the production of cytokines is influenced by the interaction between microglia and Aβ oligomers. The presence of Aβ oligomers stimulates microglia to produce cytokines up to a certain limit, that is, h_I is increasing with $\lim_{A_\beta\to\infty} h_I(A_\beta) = \mu_\beta$. Moreover, $h_I(0) = 0$ and h_I' is decreasing.

Let us give a positivity and boundedness results for the solutions, ensuring that cell populations remain positive and do not grow unboundedly.

Definition (Song 2022): Let us assume Y be a set in $\mathbb{R}^n$. A dynamical system is given by

$$\dot{x} = f(t, x), \quad t \geq 0,$$

where $x(t) \in \mathbb{R}^n$ are the state variables, t is the time variable, and $f(t, x)$ is a real-valued continuous function. The set Y is called a *positively invariant set* of the dynamical system if $x(0) \in Y$ implies $x(t) \in Y$ for all $t \geq 0$.

Proposition *(Song 2022): Let the nonnegative quadrant $\mathbb{R}^n_+$ be represented as $\{x \in \mathbb{R}^n | x_i \geq 0, i = 1, 2, \ldots, n\}$. Then $\mathbb{R}^n_+$ is an invariant set with respect to the above dynamical system if any point x on the boundary of $\mathbb{R}^n_+$ holds the following condition*

$$f_{ij}(t_0, x) \geq 0, \quad j = 1, 2, \ldots, k,$$

where $x_{ij} = 0$ for $j = 1, 2, \ldots, k$.

Statement 1 A nonnegative set $\mathbb{R}^6_+ = \{(A_m, A_\beta, \tau_p, N_F, M, I) \in \mathbb{R}^6 | A_m \geq 0, A_\beta \geq 0, \tau_p \geq 0, N_F \geq 0, M \geq, I \geq 0\}$ is an invariant set with respect to the dynamical system (1) if any point $(A_m, A_\beta, \tau_p, N_F, M, I)$ on the boundary of $\mathbb{R}^6_+$ holds the following condition

$$f_i(0, A_m, A_\beta, \tau_p, N_F, M, I) \geq 0,$$

for $i = 1, 2...6$, where $A_m = 0, A_\beta = 0, \tau_p = 0, N_F = 0, M = 0, I = 0$, respectively.

Statement 2 All the solution of the system (1) are bounded.

Proofs of positivity and boundedness for the solutions are given in Appendix A.

3 Steady States and their Stability

In this section, we find biologically feasible steady states of the system (1) and discover the dynamical nature of the same. To obtain the equilibria, we need to solve the system of equations:

$$\begin{aligned} A_m r(A_m) + A_m f(I) - h(A_m) &= 0, \\ h(A_m) - s(M)A_\beta - \delta_\beta A_\beta &= 0, \\ \gamma_p A_\beta - \delta_p \tau_p - g(\tau_p) &= 0, \\ g(\tau_p) - \delta_N N_F &= 0, \\ \gamma_M - \delta_M M + (f_M(A_\beta) + g_M(N_F))(\tilde{M} - M)M &= 0, \\ h_I(A_\beta)M - \delta_I I &= 0. \end{aligned} \tag{3}$$

3.1 Existence and Stability of Disease-free Equilibrium

A straight forward calculation leads to the existence of a unique disease-free equilibrium $(0, 0, 0, 0, \frac{\gamma_M}{\delta_M}, 0)$ of the system (1).

For examining the stability nature of the system (1), we employ the Jacobian matrix

$$\begin{pmatrix} L_1 & 0 & 0 & 0 & 0 & A_m f'(I) \\ h'(A_m) & -s(M) - \delta_\beta & 0 & 0 & -s'(M)A_\beta & 0 \\ 0 & \gamma_p & -\delta_p - g'(\tau_p) & 0 & 0 & 0 \\ 0 & 0 & g'(\tau_p) & -\delta_N & 0 & 0 \\ 0 & f'_M(A_\beta)(\tilde{M} - M)M & 0 & L_2 & L_3 & 0 \\ 0 & h'_I(A_\beta)M & 0 & 0 & h_I(A_\beta) & -\delta_I \end{pmatrix},$$

where $L_1 = A_m r'(A_m) + r(A_m) + f(I) - h'(A_m)$, $L_2 = g'_M(N_F)(\tilde{M} - M)M$, and $L_3 = -\delta_M + (f_M(A_\beta) + g_M(N_F))(\tilde{M} - 2M)$.

The eigenvalues are r_m, $-s(\frac{\gamma_M}{\delta_M}) - \delta_\beta$, $-\delta_p$, $-\delta_N$, $-\delta_M$ and $-\delta_I$. Since, $r_m > 0$, this implies that the disease-free equilibrium is unstable.

3.2 Existence of Disease Equilibrium

Theorem 1 *The system (1) admits at least one biologically feasible disease equilibrium (A^*_m, A^*_β, τ^*_p, N^*_F, M^*, I^*) if the following condition holds*

$$(\tilde{M}\delta_M - 2\gamma_M)B(K) + \delta_M \sqrt{\left(B(K)\tilde{M} - \delta_M\right)^2 + 4\gamma_M B(K)} > \delta_M^2,$$

for $\tau_p < K (> 0)$.

Proof The proof is given in Appendix B. □

4 The Mathematical Model with its Functional Forms

In the earlier sections, we have examined the model in its general expression of nonlinearities (Khajanchi 2021; Khajanchi and Banerjee 2017). Further analysis of this general form is quite challenging. Hence, to investigate deeper the dynamical behavior of the model (1), we conduct direct calculations and explore numerical solutions by replacing the nonlinear functions in system (1) with explicit expressions. These specific choices are based on their biological relevance (Section 2) and are aligned with the properties outlined in Subsection 2.4. The forms of the functions in the mathematical model (1) can be taken as

$$r\left(A_m\right)=\frac{r_m}{k_m}\left(k_m-A_m\right),\ f(I)=\frac{\mu_I I}{\alpha_I+I},\ h\left(A_m\right)=\mu_m A_m^3,\ g\left(\tau_P\right)=\mu_p\tau_p^2,$$
$$s(M)=\frac{\mu_M M}{1+\alpha_M M},\ f_M\left(A_\beta\right)=C_M A_\beta,\ g_M\left(N_F\right)=C_N N_F,\ h_I\left(A_\beta\right)=\frac{\mu_\beta A_\beta}{\alpha_\beta+A_\beta}.$$

Once we substitute the functional forms into the mathematical model (1), the resulting model is as follows:

$$\begin{cases}\dfrac{dA_m}{dt}=\dfrac{r_m A_m}{k_m}\left(k_m-A_m\right)+\dfrac{\mu_I A_m I}{\alpha_I+I}-\mu_m A_m^3,\\ \dfrac{dA_\beta}{dt}=\mu_m A_m^3-\dfrac{\mu_M A_\beta M}{\alpha_M M+1}-\delta_\beta A_\beta,\\ \dfrac{d\tau_p}{dt}=\gamma_p A_\beta-\delta_p\tau_p-\mu_p\tau_p^2,\\ \dfrac{dN_F}{dt}=\mu_p\tau_p^2-\delta_N N_F,\\ \dfrac{dM}{dt}=\gamma_M-\delta_M M+(C_M A_\beta+C_N N_F)(\tilde{M}-M)M,\\ \dfrac{dI}{dt}=\dfrac{\mu_\beta A_\beta M}{\alpha_\beta+A_\beta}-\delta_I I,\end{cases}\tag{4}$$

with the initial condition $A_m(0)\geq 0$, $A_\beta(0)\geq 0$, $\tau_p(0)\geq 0$, $N_F(0)\geq 0$, $M(0)\geq 0$ and $I(0)\geq 0$.

All parameters of the model (4) are positive and their corresponding descriptions are given in Table 1.

We have already determined the steady states for the generalized mathematical model (4) which is given in Section 3. We get two equilibria: disease-free equilibrium and disease equilibrium. As mentioned previously, the disease-free equilibrium $(0,0,0,0,\frac{\gamma_M}{\delta_M},0)$ is unstable. The disease equilibrium can be represented as

Table 1 Descriptions of parameters of the model (4)

Parameters	Descriptions	Baseline values	References	Ranges
r_m	Growth rate of Aβ monomers	$7.49326h^{-1}$	Fitted	[5.620, 9.3665]
k_m	Carrying capacity of Aβmonomers	125.721μM	Fitted	[94.281, 157.161]
μ_I	Activation production rate of Aβ monomer by TNF-α	$6.18925h^{-1}$	Fitted	[4.642, 7.736]
α_I	Saturation coefficient of TNF-α	2.51104μM	Fitted	[1.883, 3.139]
μ_m	Conversion rate from Aβmonomers to Aβoligomers	$0.000618h^{-1}\mu\text{M}^{-2}$	Fitted	[0.000464, 0.000773]
μ_M	Clearance rate of Aβoligomers due to microglia	$5.01579cells.mm^{-3}h^{-1}$	Fitted	[3.762, 6.269]
α_M	Saturation coefficient of microglia	8.50706×10^{-6}	Fitted	$[6.380 \times 10^{-6}, 1.0635 \times 10^{-6}]$
δ_β	Degeneration rate of Aβoligomers	$0.3465h^{-1}$	Estimated	[0.2599, 0.4330]
γ_p	Phosphorylation rate of$\tau$by Aβ oligomers	$0.00020373\mu\text{M}h^{-1}n\text{M}^{-1}$	Fitted	[0.0001528, 0.0002546]
δ_p	Degeneration rate ofτprotein	$0.0012h^{-1}$	Estimated	[0.0009, 0.0015]
μ_p	Conversion rate fromτmonomer to NFTs	$0.170351h^{-1}\mu\text{M}^{-1}$	Fitted	[0.1278, 0.2129]
δ_N	Degeneration rate of NFTs	$6.49667h^{-1}$	Fitted	[4.8725, 8.1208]
γ_M	Proliferation rate of microglia	$0.2532cells.mm^{-3}.h^{-1}$	Estimated	[0.1899, 0.3165]
δ_M	Degeneration rate of microglia	$0.0000634h^{-1}$	Estimated	[0.0000476, 0.0000792]
C_M	Activation rate of microglia by Aβ oligomers	$0.000095h^{-1}$	(Hao and Friedman 2016)	[0.0000713, 0.0001188]
C_N	Activation rate of microglia by NFTs	$0.00833h^{-1}$	(Hao and Friedman 2016)	[0.00625, 0.01042]
$\tilde{M}$	Maximum capacity of microglia	$1cells.mm^{-3}$	(Ciuperca et al. 2024)	[0.75, 1.25]
μ_β	Production rate of TNF-$\alpha$by Aβ oligomers	$0.0012\mu\text{M } mm^3h^{-1} \ cells^{-1}$	(Hao and Friedman 2016)	[0.0009, 0.0015]
α_β	Saturation coefficient of Aβ oligomers	$2.68854n$M	Fitted	[2.016, 3.361]
δ_I	Degeneration rate of TNF-α	$9.041h^{-1}$	Estimated	[6.781, 11.302]

$$A_\beta = \frac{\delta_p \tau_p + \mu_p \tau_p^2}{\gamma_p}, \quad N_F = \frac{\mu_p \tau_p^2}{\delta_N},$$
$$M = \frac{\tilde{M}\alpha - \delta_M + \sqrt{(\tilde{M}\alpha - \delta_M)^2 + 4\alpha\gamma_M}}{2\alpha}, \text{ where } \alpha = C_M A_\beta + C_N N_F,$$

and

$$I = \frac{\mu_\beta A_\beta M}{(\alpha_\beta + A_\beta)\delta_I}.$$

We clearly observe that A_β, N_F, M and I can be defined in terms of A_m and τ_p, where A_m and τ_p are the solution of the below system:

$$\tilde{f}(A_m, \tau_p) = \frac{r_m}{k_m}(k_m - A_m) + \frac{\mu_I I}{\alpha_I + I} - \mu_m A_m^2 = 0, \tag{5}$$

$$\tilde{g}(A_m, \tau_p) = \mu_m A_m^3 - \frac{\mu_M A_\beta M}{\alpha_M M + 1} - \delta_\beta A_\beta = 0. \tag{6}$$

Finding an explicit analytical solution for this system is somewhat challenging due to its complexity. To ensure the existence of equilibria, we have given a graphical representation in numerical section (Fig. 3). This figure illustrates the existence of equilibrium points by showing the intersection of two surfaces, given by (5)-(6), in the (A_m, τ_p) plane, where τ_p and A_m represent the τ protein and Aβ monomer concentration, respectively. The figure and corresponding details are given in numerical section.

5 Numerical Simulation

Parameters and their corresponding values play a significant role in the field of mathematical biology. By having the intention to get biological equivalent parameter values, in this section, we estimate them using two methods: (i) directly from the literature and (ii) through data fitting based on published data. Using these parameter values, we validate analytical results further. Combining the UA with Partial Rank Correlation Coefficient (PRCC), we check the sensitivity of our model output with respect to the model parameters. We apply the standard LHS-PRCC scheme and draw the scatter plots with correlation index, PRCC, and also provide the respected p-values.

5.1 Literature-derived Parameter Estimation

In this subsection, we gather data from various scientific or clinical studies and papers to determine the values of parameters involved in the mathematical model. The parameters of the model are estimated as follows:

Estimation of δ_M: The half life of microglia is approximately 15 months (Fuger et al. 2017; Vidal-Itriago et al. 2022), which is equal to 1.0957×10^4 hours (h). Hence the degeneration rate of microglia can be calculated as

$$\delta_M = \frac{\ln 2}{1.0957 \times 10^4}\ h^{-1} = 0.633 \times 10^{-4}\ h^{-1}.$$

Estimation of γ_M: The density of microglia is 3000-9000 $cells.mm^{-3}$ (Keller et al. 2018). For healthy brain, the steady state of microglia from the fifth equation of the model (4) is $\gamma_M - \delta_M M = 0$. Let us assume the density as 4000 $cells.mm^{-3}$. Hence, the growth rate of microglia can be calculated as $\gamma_M = \delta_M M = 4000 \times 0.633 \times 10^{-4}\ cells.mm^{-3}.h^{-1} = 0.2532\ cells.mm^{-3}.h^{-1}$.

Estimation of δ_I: The half life of TNF-α is 4.6 *min* (Simo et al. 2012; Lai et al. 2020). The degeneration rate of TNF-α is

$$\frac{\ln 2}{0.076667} = 9.04104\ h^{-1}.$$

Estimation of δ_β: The majority of Aβ oligomers has half life 1–5 h (Dear et al. 2020). Let us take, the half life is 2 h, hence the degeneration rate is calculated as

$$\frac{\ln 2}{2} = 0.3465\ h^{-1}.$$

Estimation of δ_p: The half life of τ protein in the brain is 552 h (Hier et al. 2022). The degeneration rate can be determined by

$$\frac{\ln 2}{552} = 0.0012\ h^{-1}.$$

5.2 Data-driven Parameter Estimation

This subsection focuses on estimating the rest of the parameters through data fitting (Banerjee et al. 2015). The key factors in AD are the misfolding and the aggregation of proteins into oligomers and fibrillar structures. Here, we concentrate on fitting the data for Aβ oligomers concentration and τ protein concentration across time. We try to find good estimate of the parameters k_m, r_m, μ_I, α_I, μ_m, μ_M, α_M, γ_p, μ_p, δ_N and α_β of the mathematical model (4).

We fit the variables to the experimental data using a nonlinear least-squares optimization approach. This approach was selected due to the inherent nonlinearity in our model. The fitting process was conducted using NonlinearModelFit algorithm in Mathematica software. This function optimizes the model parameters by minimizing the sum of squared residuals between the observed data and the model's predictions. Although the number of observed data points was fewer compared to the complexity of the model and parameters, we tried to achieve the best possible fit. In such a scenario, the fitting process becomes a little challenging.

We have adapted the Aβ oligomers concentration data and τ protein concentration data from the papers by Dear et al. (2020, 2020). The data points displayed in Fig. 2(a) for Aβ oligomer concentration are sourced from Fig. 6(a) (page 6242) in Dear et al. (2020), while the data points shown in Fig. 2(b) for τ protein concentration are obtained from Fig. 8(a) (page 6244) in Dear et al. (2020). The data used in the study was obtained from in vitro experiments, conducted in controlled laboratory conditions using experimental techniques such as single-molecule fluorescence resonance energy transfer (FRET) and induced aggregation reactions. In Fig. 2, the red data points indicate the observed concentrations of Aβ oligomers and τ protein over time, and the curves represent the model's fit to these experimental results. The estimated parameter values are given in Table 1 columnized as baseline values.

5.3 Model Validation and Primary Analysis

Figure (3) shows the existence of disease-free equilibrium and the disease equilibrium for the parameter values given in Table 1. In Fig. 3, two interaction points are shown in the (τ_p, A_m) plane, where τ_p and A_m denote the τ protein and Aβ monomer population, respectively. The red surface corresponds to the function $\tilde{g}(\tau_p, A_m) = 0$, whereas the blue surface corresponds to the function $\tilde{f}(\tau_p, A_m) = 0$. The equilibrium points of the system are obtained at the intersections of these two surfaces. This confirms the existence of two equilibria (0, 0, 0, 0, 3993.69, 0) and (72.0064, 0.793138, 0.0274771, 0.0000198, 57.986, 0.00175) of the system (4). We have taken a set of initial points from where all the trajectories are starting as $A_m(0) = 70$, $A_\beta(0) = 0.79$, $\tau_p(0) = 0.02$, $N_F(0) = 0.00001$, $M(0) = 57$, $I(0) = 0.001$.

In Fig. 4, we have plotted the temporal dynamics of the population of Aβ protein oligomers and NFTs, taking into account the influence of the immune response (microglia population) on them. For plotting the figure, we have taken two cases: higher activation rates with lower proliferation rate of microglia and lower activation rates with higher proliferation rate of microglia. In the plots, the red curves represent

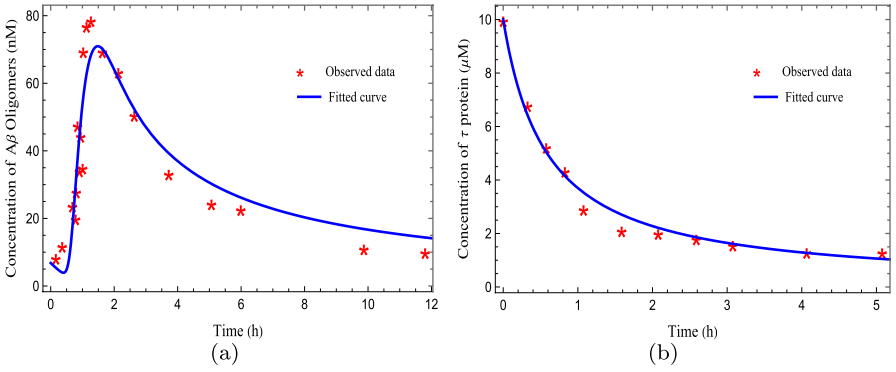

Fig. 2 Data points are used to estimate the parameters $k_m, r_m, \mu_I, \alpha_I, \mu_m, \mu_M, \alpha_M, \gamma_p, \mu_p, \delta_N$ and α_β in the mathematical model (4). The figure (**a**) describes the data and corresponding best fit curve for the population of Aβ oligomers and (**b**) describes the data and corresponding best fit curve for the population of τ protein. Source of data: (Dear et al. 2020, 2020)

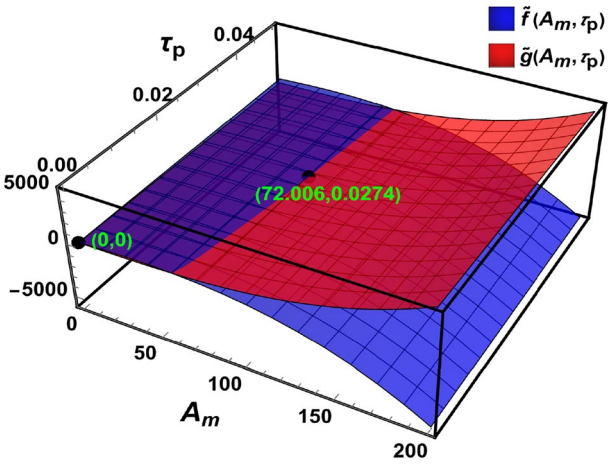

Fig. 3 Graphical representation of the existence of equilibria of the system (4) in the (τ_p, A_m) plane, where τ_p and Aβ monomer population, respectively

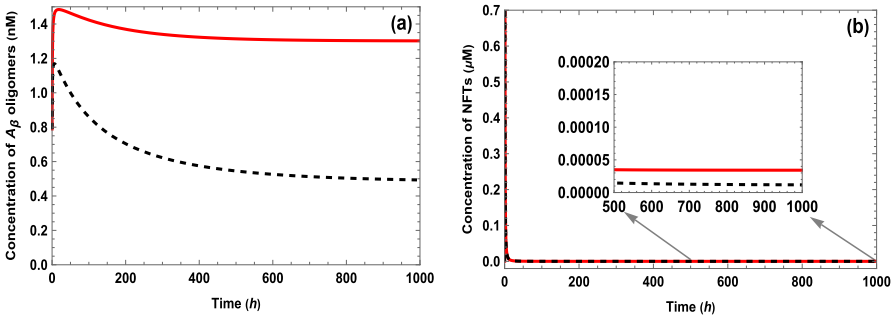

Fig. 4 Temporal dynamics of Aβ oligomers and NFTs under different activation and proliferation rates of microglia. The red curves correspond to the rates $C_M = 0.0001188$, $C_N = 0.01042$, $\gamma_M = 0.1899$, while the black curves correspond to the rates $C_M = 0.0000713$, $C_N = 0.00625$, $\gamma_M = 0.3165$. Other parameter values are given in Table 1

the first case (C_M = 0.0001188, C_F = 0.01042, γ_M = 0.1899), whereas the black curves define the second case (C_M = 0.0000713, C_N = 0.00625, γ_M = 0.3165). The other parameters values are taken from Table 1. When the proliferation rate of microglia is high and the activation rates of microglia are low, the both of Aβ oligomers and NFTs population decreases.

5.4 Uncertainty and Sensitivity Analysis

To capture the most sensitive parameters of this complex mathematical model (4), we find the Partial Rank Correlation Coefficient (PRCC). To get a clearer understanding of the parameters sensitivity, we examine scatter plots depicting the relationships between model variables and individual parameters. Remind that PRCC is a statistical technique used to measure the sensitivity of model outputs to changes in input

(Zi 2011; Savatorova 2023). Generally, PRCC values range from −1 to 1, with values closer to −1 or 1 indicating stronger negative or positive correlations, respectively. A scatter plot is a dot graph used to display the relationship between two variables. Patterns in the distribution of points are useful for identifying correlations between the variables (Hastie et al. 2017; Iooss and Lemaitre 2015).

We have taken the baseline parameters values from Table 1 and the range of the parameters are considered in 25% intervals of the baseline values. For generating PRCC and scatter plots, we used an inspired MATLAB code provided by Marino et al. (2008).

We perform PRCC analysis at four different time points to investigate which input variables (model parameters) have a great influence on the output variables (model populations). The four different time points that have been taken, are $t = 100\ h$, $200\ h$, $300\ h$ and $400\ h$, and for doing this sensitivity analysis the sample size is set to 2000. In our model, we are mainly interested in investigating the parameter influence on two important populations Aβ oligomers (A_β) and NFTs (N_F).

Figure 5 shows the PRCC plot for the protein population of Aβ oligomers at different time points t= 100 h, 200 h, 300 h and 400 h. These four time points have been picturised in four slots 1, 2, 3 and 4, respectively. A color chart is attached which shows the color indicter and corresponding parameters. In Fig. 5, PRCC results show how the parameters r_m, k_m, μ_m, μ_M, γ_M, C_M and $\tilde{M}$ are consistently significant and most important parameters for the population of Aβ oligomers. It suggests that the dynamics of the population of Aβ oligomers is strongly affected by the variation of parameters r_m, k_m, μ_m, μ_M, γ_M, C_M and $\tilde{M}$. PRCC scatter plots are also produced for the Aβ oligomers with respect to these parameters.

In Fig. 6, the axes indicate the residuals of the linear regression between the rank-transformed values of the Aβ population against the rank-transformed values of each of the parameters. Here, we consider that the parameters are statistically significant with the significance value 0.05. The growth rate r_m and carrying capacity k_m of Aβ monomer have a strong positive correlation (PRCC 0.89934 and 0.94453) with the A_β population (Fig. 6(a) and (b)). This suggests that as the rates at which Aβ mono-

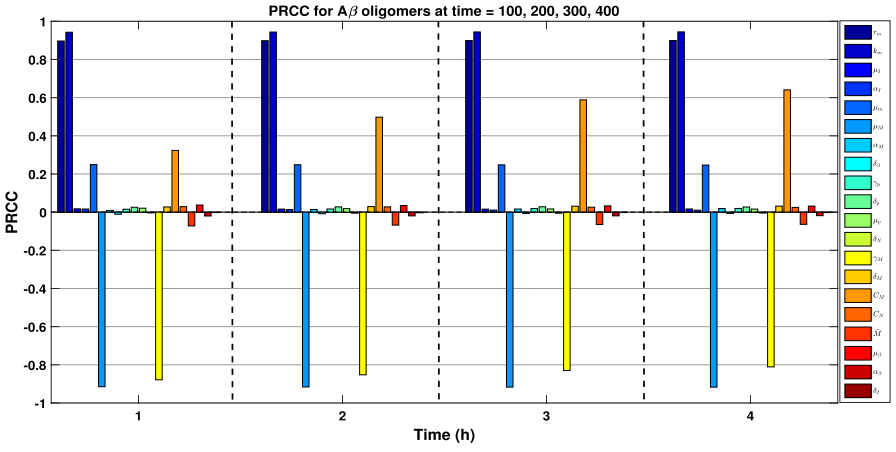

Fig. 5 PRCC results for the Aβ oligomers at four different times t= 100, 200, 300, 400 h

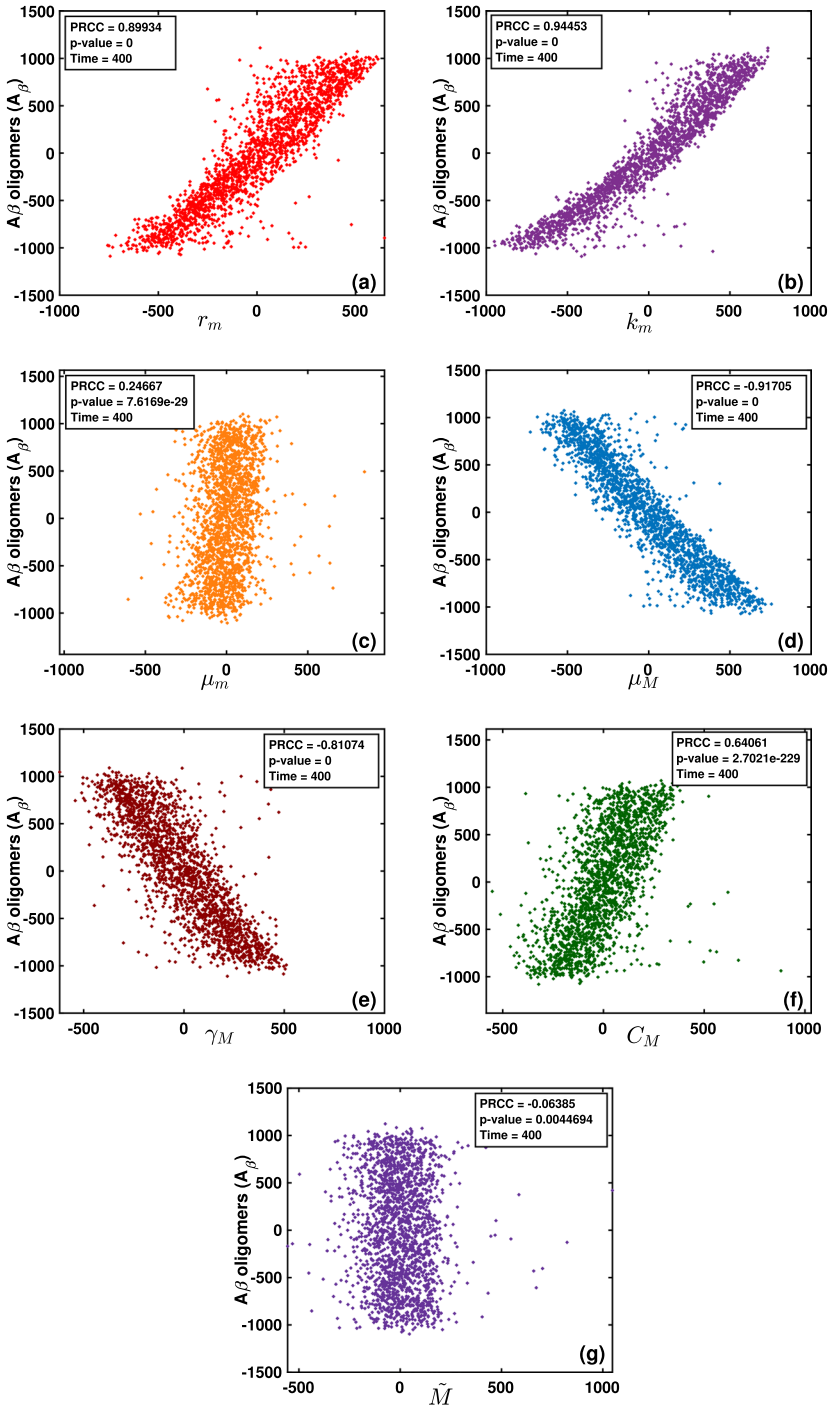

Fig. 6 Scatter plot showing the relationship between Aβ oligomer population and the parameters: PRCC and the corresponding p-values of the parameters **(a)** r_m, **(b)** k_m, **(c)** μ_m, **(d)** μ_M, **(e)** γ_M, **(f)** C_M, **(g)** $\tilde{M}$ for the population Aβ oligomers at time $t = 400\ h$

mers produce increases, the number of Aβ oligomers also increases significantly. We can see in Fig. 6(c), the parameter μ_m, conversion rate from Aβ monomers to oligomers, has a moderate positive correlation with A_β population as the PRCC value is 0.24667 and p-value 7.6169e-29 < 0.05. The parameters with large absolute PRCC values, PRCC $> |0.5|$, with corresponding p-values ≤ 0.05, are considered to be the most important parameters (Nagaraja et al. 2019; Taylor 1990). The A_β population has the strong negative correlation with the parameters μ_M (the clearance rate of Aβ oligomers) and γ_M (proliferation rate of microglia), with PRCC values −0.91705 and −0.81704, respectively (Fig. 6(d) and (e)). This indicates that a decrease in the parameters μ_M and γ_M, governed by the microglia population, is associated with an increase in the Aβ oligomer population. The parameter C_M, activation rate of microglia by Aβ oligomers, has a positive correlation with the A_β population with the PRCC value 0.64061 (Fig. 6(f)). While the correlation is positive, it is not as strong as in some other cases, indicating that C_M plays a significant but not dominant role. The parameter $\tilde{M}$ has a weak negative correlation with the Aβ oligomers population as the PRCC value is −0.06385 and the p-value is 0.0044694 < 0.05 (Fig. 6(g)). That suggests statistical significance but the strength of the correlation is relatively low. This weak correlation suggests that variations in the maximum capacity of microglia, $\tilde{M}$ have a minimal effect on the population of Aβ oligomers. Other parameters μ_I, α_I, α_M, δ_β, γ_p, δ_p, μ_p, δ_N, δ_M, C_N, μ_β, α_β and δ_I have very minimal PRCC values and p-values are greater than 0.05. This suggests that changes in these parameters have an almost negligible influence on the population of Aβ oligomers.

Figure 7 shows the PRCC plot for the protein population of neurofibrillary tangles (N_F) at different time points t= 100 h, 200 h, 300 h and 400 h. The consistently significant parameters for N_F population are r_m, k_m, μ_m, μ_M, γ_p, δ_p, μ_p, δ_N, γ_M, C_M and $\tilde{M}$. Hence, the variation of these parameters mainly impacts the protein population N_F. For a graphical visualization, PRCC scatter plot are also given for N_F with relative to the significant parameters.

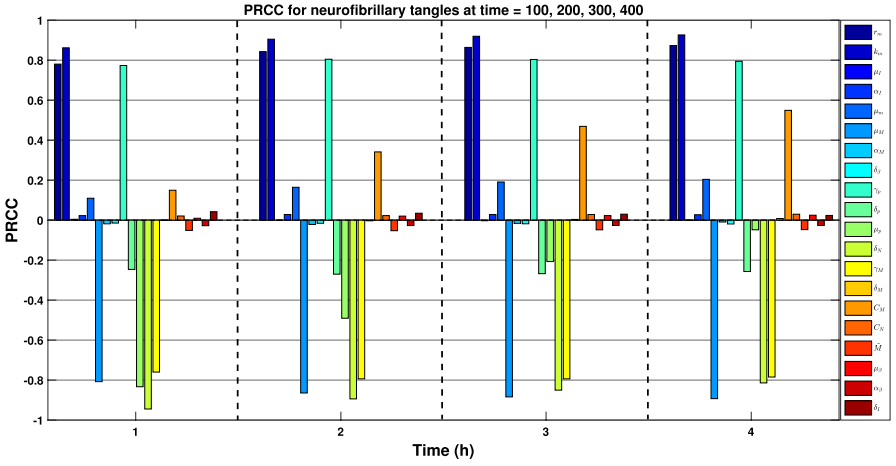

Fig. 7 PRCC results for the neurofibrillary tangles at four different times t = 100, 200, 300, 400 h

Here, we have taken the statistically significance value at 0.05. The growth rate r_m and carrying capacity k_m of Aβ monomer have a strong positive correlation (PRCC 0.87318 and 0.9263, respectively) with the N_F population (Fig. 8(a) and (b)). This strong correlation indicates that variations in two parameters r_m and k_m, are crucial in affecting the NFTs population. Remind that parameters with large absolute PRCC values, PRCC $> |0.5|$, with corresponding p-values < 0.05, are considered to be the most important parameters (Nagaraja et al. 2019; Taylor 1990). Besides r_m and k_m, the parameters μ_m, μ_M, γ_p, δ_N, γ_M, δ_p, μ_p, $\tilde{M}$ and C_M are also significant and have impact on the NFTs population (see Fig. 8). Rather than the significant parameters, there are many parameters that have very less impact on the NFTs population, which is negligible. The parameters μ_I, α_I, α_M, δ_β, δ_M, C_N, μ_β, α_β and δ_I has less PRCC value and p-value > 0.05.

6 Discussion and Conclusion

In this paper, we have formulated a mathematical model based on the events: aggregation of proteins, activation of immune cells and initiation of inflammation. Aggregation of proteins (Aβ plaque and NFTs) has been recognized as a hallmark in the progression of AD since its discovery. Having a critical relevance to AD, our model includes two key disease-related proteins along with their aggregated forms. Microglia, which have an intricate involvement in AD, are known to regulate both phagocytosis and inflammatory responses (Miao et al. 2023). In early activation, microglia primarily contribute to the clearance of oligomers, while with prolonged activation, they tend to shift toward a pro-inflammatory phenotype and release cytokines. For tractability, we adopted the simplified formulation where each activated microglial cell contributes to both processes. Recognizing the significance of microglia and inflammation in the progression of AD, we have included both microglia and cytokines as components of our model. We believe that our model generalizing the existing ones, provides flexibility and is able to capture realistic biological dynamics.

After formulating the mathematical model, we have conducted an extensive review of both biological and mathematical literature to identify the relevant properties of the functional forms. This exploration allowed us to choose functional forms that not only represent the underlying biological processes but also follow mathematical principles.

We have investigated the fundamental properties of our mathematical model and analyzed its dynamical behavior by identifying the equilibrium points. Once the equilibria are determined, stability analysis have been performed to understand the system's behavior near these points. The disease-free equilibrium is always unstable, implying that once pathological processes begin, the system cannot recover to a completely normal state. This is consistent with the largely irreversible character of AD, while early-stage protective mechanisms may reverse the progression.

Due to the complexity of the model, determining the exact form of the disease equilibrium was challenging. However, through mathematical calculations and numerical simulation, we have demonstrated the existence of a disease equilibrium for the system.

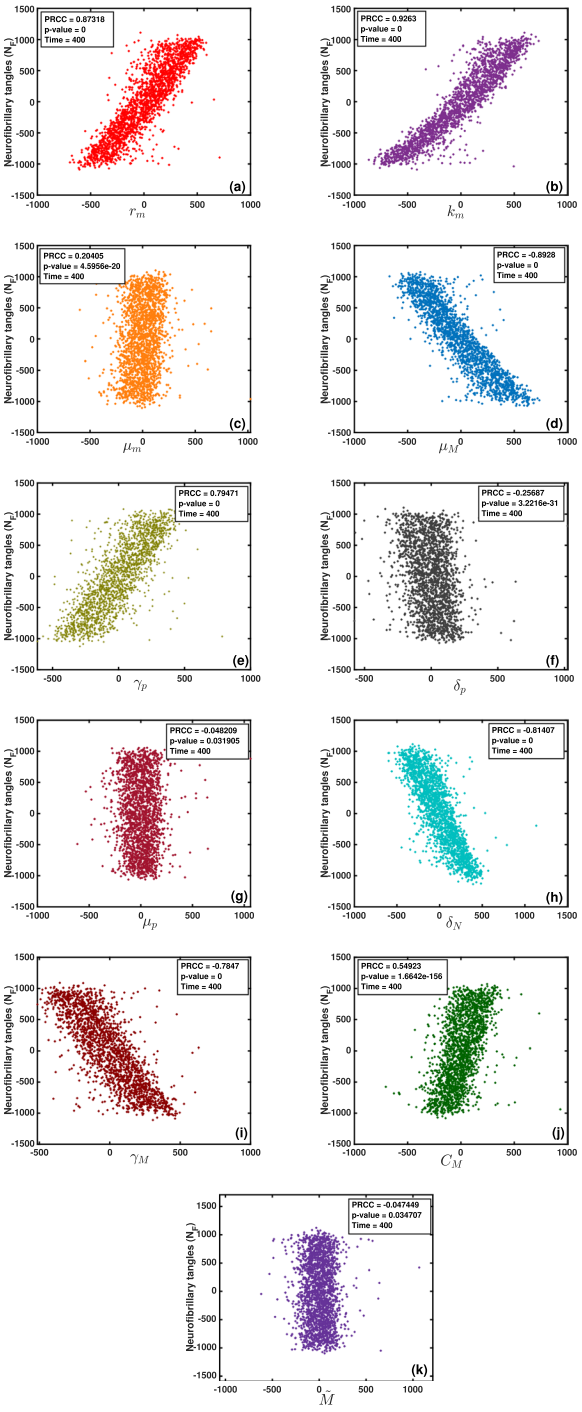

Fig. 8 Scatter plots showing the relationship between NFTs population and the parameters: PRCC and the corresponding p-values of the parameters (**a**) r_m, (**b**) k_m, (**c**) μ_m, (**d**) μ_M, (e) γ_p, (**f**) δ_p, (**g**) μ_p, (**h**) δ_N, (**i**) γ_M, (**j**) C_M, (**k**) $\bar{M}$ for the population NFTs population at time $t = 400h$

When we formulated the generalized mathematical model, some basic properties of the functions were assumed. Based on the biological significant assumptions, we have considered the explicit forms of the model.

In numerical solutions, we have done the parameter estimation through two methods: from biological literature and data fitting. To improve the model's predictive power, we have performed the data fitting on Aβ oligomer and τ protein datasets to calibrate some of the model parameters. The timescale in our model is determined by the experimental data used for parameter estimation, which were available in hours (Dear et al. 2020, 2020). Considering the estimated values as baseline values of the parameters, we have identified key parameters that significantly influence the model's output through the SA and UA. This allows us to choose which factors we should focus on for more accurate predictions and a deeper understanding of the system's dynamics. To understand the scenario globally, we have taken the help of PRCC determination and scatter plots. In PRCC plot, we compared the situations at four different time points 100 *h*, 200 *h*, 300 *h* and 400 *h*.

The production or growth of Aβ monomer, that is, the growth rate r_m and the carrying capacity k_m has a positive impact on both the Aβ oligomer and NFTs population. Since in both the cases, we have seen that the PRCC values are > 0.8 implies a strong positive correlation between the parameters and model populations. Also observing the scatter plots, we conclude that increase in growth factors of Aβ monomer, leads to increase in both Aβ oligomer and NFTs population.

In the Fig. 8(e), we note that the phosphorylation rate γ_p has a strong positive correlation with NFTs population. As the rate of phosphorylation (γ_p) increases, there is a corresponding rise in the NFTs population. This fact aligns with the well-established biological fact that NFTs formation is heavily influenced by the phosphorylation of τ protein. The increased phosphorylation leads to more τ proteins becoming dysfunctional and forming NFTs, which helps in AD progression. Hence, the figure highlights the critical role of phosphorylation in NFT formation and AD advancement.

The two parameters μ_M and γ_M, related to microglia, have a strong negative correlation with both the Aβ oligomers and NFTs. From this, we can conclude that as the saturation and proliferation of microglia increase, the levels of Aβ oligomers and NFTs tend to decrease. This suggests that microglial activity may play a significant role in reducing the accumulation of these pathological biomarkers.

In this work, the application of SA related to UA is employed to identify the parameters with the highest sensitivity regarding the progression of AD. PRCC helps researchers understand which parameters are most critical in their models, guiding further research, data collection efforts and model refinement.

Limitations of this work: the model faces limitations, such as the exclusion of nucleation, elongation and fragmentation processes, which may limit its representation of Aβ aggregation. Another limitation is that our model does not explicitly include dissociation of monomers from oligomers. Additionally, only microglia has been considered as a immune system in our model which might not fully capture the complexity of neuroinflammation in AD. The absence of spatial dynamics in the model may limit its relevance to the progression of diseases in specific regions. We have not gone through the complete τ propagation mechanisms.

Future directions: for future directions, several extensions can be explored to enhance the current model of AD. Spatial dynamics can be incorporated into the model. Additionally, including nucleation, elongation and fragmentation processes could provide a more comprehensive view of Aβ aggregation and its impact on disease outcomes. To finding treatment strategies, optimal control theory can be used.

Appendix A: Positivity and boundedness of the model

Proof of statement 1

Proof Let us consider

$$\begin{aligned}
&f_1(0, A_m, A_\beta, \tau_p, N_F, M, I) = A_m r(A_m) + A_m f(I) - h(A_m),\\
&f_2(0, A_m, A_\beta, \tau_p, N_F, M, I) = h(A_m) - s(M)A_\beta - \delta_\beta A_\beta,\\
&f_3(0, A_m, A_\beta, \tau_p, N_F, M, I) = \gamma_p A_\beta - \delta_p \tau_p - g(\tau_p),\\
&f_4(0, A_m, A_\beta, \tau_p, N_F, M, I) = g(\tau_p) - \delta_N N_F,\\
&f_5(0, A_m, A_\beta, \tau_p, N_F, M, I) = \gamma_M - \delta_M M + (f_M(A_\beta) + g_M(N_F))(\tilde{M} - M)M,\\
&f_6(0, A_m, A_\beta, \tau_p, N_F, M, I) = h_I(A_\beta)M - \delta_I I.
\end{aligned} \tag{7}$$

Now, for $A_m = 0$, $f_1 = 0$, for $A_\beta = 0$, $f_2 = h(A_m) \geq 0$, for $\tau_p = 0$, $f_3 = \gamma_p A_\beta \geq 0$, for $N_F = 0$, $f_4 = g(\tau_p) \geq 0$, for $M = 0$, $f_5 = \gamma_M \geq 0$, for $I = 0$, $f_6 = h_I(A_\beta)M \geq 0$.

This proves that $\mathbb{R}^6_+$ is an invariant set with respect to the dynamical system (1). Hence for, $A_m(0) \geq 0$, $A_\beta(0) \geq 0$, $\tau_p(0) \geq 0$, $N_F(0) \geq 0$, $M(0) \geq 0$, $I(0) \geq 0$, then $A_m(t) \geq 0$, $A_\beta(t) \geq 0$, $\tau_p(t) \geq 0$, $N_F(t) \geq 0$, $M(t) \geq 0$, $I(t) \geq 0$.

□

Proof of statement 2

Proof The solutions of the system have the following properties:

- The maximum value of the term $f(I)$ is μ_I. The first equation of model (1) can be written as $\frac{dA_m}{dt} \leq A_m r(A_m) + A_m f(I)$. In absence of inflammation, the maximum value of A_m will be k_m, the carrying capacity for Aβ monomer population. But, here $f(I)$ positively influences the production of Aβ monomer, it could allow the population to reach a higher maximum size than the carrying capacity. Moreover, $\frac{dA_m}{dt} \leq A_m(r(A_m) + \mu_I)$. Hence the maximum value of A_m could be $(A_m)_{\max} = b\ k_m$, where $b > 0$ is a constant. We can determine the constant b depending on the specific form of the expressions.
- For the variable A_β, $\frac{dA_\beta}{dt} \leq h(bk_m) - \delta_\beta A_\beta$ which implies the maximum value of A_β is $(A_\beta)_{\max} = \max\left\{\frac{h(bk_m)}{\delta_\beta}, A_\beta(0)\right\}$.
- In the third equation, $\frac{d\tau_p}{dt} \leq \gamma_p (A_\beta)_{\max} - \delta_p \tau_p$ implies

$\tau_p \leq (\tau_p)_{\max} = \max\left\{\frac{\gamma_p (A_\beta)_{\max}}{\delta_p}, \tau_p(0)\right\} = K(say)$.

- For the variable N_F, $\frac{dN_F}{dt} \leq g((\tau_p)_{\max}) - \delta_N N_F$ implies $N_F \leq (N_F)_{\max} = \max\left\{\frac{g((\tau_p)_{\max})}{\delta_N}, N_F(0)\right\}$.
- In the fifth equation, $\frac{dM}{dt} \leq \gamma_M - \delta_M M + ((A_\beta)_{\max} + (N_F)_{\max})\frac{\tilde{M}^2}{4}$ implies $M \leq M_{\max} = \max\left\{\frac{((A_\beta)_{\max}+(N_F)_{\max})\tilde{M}^2+4\gamma_M}{4\delta_M}, M(0)\right\}$.
- The maximum value of the term $h_I(A_\beta)$ is μ_I. Hence, $\frac{dI}{dt} \leq \mu_I M_{\max} - \delta_I I$ implies $I \leq I_{\max} = \max\left\{\frac{\mu_I M_{\max}}{\delta_I}, I(0)\right\}$. □

Appendix B: Existence of disease equilibrium

Proof of Theorem 1 The disease equilibrium is given by $(A_m^*, A_\beta^*, \tau_p^*, N_F^*, M^*, I^*)$ where

$$A_\beta^* = \frac{\delta_p \tau_p^* + g(\tau_p^*)}{\gamma_p}, \quad N_F^* = \frac{g(\tau_p^*)}{\delta_N}, \quad I^* = \frac{h_I(A_\beta^*)M^*}{\delta_I}.$$

To find the value of M^*, we solve the fifth equation of the system (3)

$$B(\tau_p^*)M^{*2} - (B(\tau_p^*)\tilde{M} - \delta_M)M^* - \gamma_M = 0, \tag{8}$$

where

$$B(\tau_p^*) = f_M(A_\beta^*) + g_M(N_F^*) = f_M\left(\frac{\delta_p \tau_p^* + g(\tau_p^*)}{\gamma_p}\right) + g_M\left(\frac{g(\tau_p^*)}{\delta_N}\right).$$

It is clear that equation (8) has always one positive root regardless any conditions. The solution is

$$M^* = \frac{(B(\tau_p^*)\tilde{M} - \delta_M) + \sqrt{(B(\tau_p^*)\tilde{M} - \delta_M)^2 + 4B(\tau_p^*)\gamma_M}}{2B(\tau_p^*)}.$$

Now to find the disease steady states of the variables A_m and τ_p, we need to solve the first two equations

$$r(A_m^*) + f(I^*) - h(A_m^{*\frac{n-1}{n}}) = 0, \tag{9}$$

$$h(A_m^*) - s(M^*)A_\beta^* - \delta_\beta A_\beta^* = 0. \tag{10}$$

Putting the values of A_β^*, M^* and I^*, the equations (9) and (10) read as

$$f\left(\frac{h_I\left(\frac{\delta_p\tau_p^*+g(\tau_p^*)}{\gamma_p}\right)\left((B(\tau_p^*)\tilde{M}-\delta_M)+\sqrt{(B(\tau_p^*)\tilde{M}-\delta_M)^2+4B(\tau_p^*)\gamma_M}\right)}{2B(\tau_p^*)\delta_I}\right) \quad (11)$$
$$-h(A_m^{*\frac{n-1}{n}})+r(A_m^*)=0,$$

$$h(A_m^*)-\left(s\left(\frac{(B(\tau_p^*)\tilde{M}-\delta_M)+\sqrt{(B(\tau_p^*)\tilde{M}-\delta_M)^2+4B(\tau_p^*)\gamma_M}}{2B(\tau_p^*)}\right)+\delta_\beta\right) \quad (12)$$
$$\times\frac{\delta_p\tau_p^*+g(\tau_p^*)}{\gamma_p}=0,$$

Let us assume an auxiliary function $F(\tau_p)$ of the equation (12)

$$F(\tau_p)=h(A_m)-\left(s\left(\frac{(B(\tau_p)\tilde{M}-\delta_M)+\sqrt{(B(\tau_p)\tilde{M}-\delta_M)^2+4B(\tau_p)\gamma_M}}{2B(\tau_p)}\right)+\delta_\beta\right) \quad (13)$$
$$\times\frac{\delta_p\tau_p+g(\tau_p)}{\gamma_p},$$

for $A_m>0$. For every $A_m>0$, $F(0)=h(A_m)>0$ and $\lim_{\tau_p\to\infty}F(\tau_p)=-\infty$. Hence, if $F(\tau_p)$ is a decreasing function, that is, $F'(\tau_p)<0$ then for each A_m, there is exactly one positive steady state for τ_p. Now differentiating (13) with respect to τ_p, we have

$$F'(\tau_p)=$$
$$-\frac{1}{\gamma_p}\left(\left(g'(\tau_p)+\delta_p\right)\left(s\left(\frac{\sqrt{\left(B(\tau_p)\tilde{M}-\delta_M\right)^2+4\gamma_M B(\tau_p)}+B(\tau_p)\tilde{M}-\delta_M}{2B(\tau_p)}\right)+\delta_\beta\right)\right)$$
$$-\frac{1}{\gamma_p}\frac{\left(\delta_M\sqrt{\left(B(\tau_p)\tilde{M}-\delta_M\right)^2+4\gamma_M B(\tau_p)}+\tilde{M}\delta_M B(\tau_p)-2\gamma_M B(\tau_p)-\delta_M^2\right)}{2B(\tau_p)^2\sqrt{\left(B(\tau_p)\tilde{M}-\delta_M\right)^2+4\gamma_M B(\tau_p)}}$$
$$\times B'(\tau_p)\left(g(\tau_p)+\delta_p\tau_p\right)s'\left(\frac{\sqrt{\left(B(\tau_p)\tilde{M}-\delta_M\right)^2+4\gamma_M B(\tau_p)}+B(\tau_p)\tilde{M}-\delta_M}{2B(\tau_p)}\right).$$

From our assumptions, we have the properties that g, s, f_M and g_M are positive and g', s', f_M' and g_M' are increasing, decreasing, nondecreasing and nondecreasing, respectively. It follows that $F'(\tau_p)$ is decreasing when the condition holds:

$$\tilde{M}\delta_M B(\tau_p)-2\gamma_M B(\tau_p)+\delta_M\sqrt{\left(B(\tau_p)\tilde{M}-\delta_M\right)^2+4\gamma_M B(\tau_p)}>\delta_M^2. \quad (14)$$

Since $F'(\tau_p)$ is decreasing and negative, then $F(\tau_p)$ is decreasing for any $\tau_p>0$.

We have $\tau_p<K(>0)$, hence, the condition (14) can be written as

$$\tilde{M}\delta_M B(K) - 2\gamma_M B(K) + \delta_M \sqrt{\left(B(K)\tilde{M} - \delta_M\right)^2 + 4\gamma_M B(K)} > \delta_M^2. \quad (15)$$

The condition (15) is a sufficient condition ensuring that the auxiliary function $F(\tau_p)$ is decreasing on $(0,\infty)$. If the condition holds, it ensures the existence of exactly one positive root $\tau_p^* > 0$ and hence a unique disease equilibrium within the system. This means it determines whether a stable state may be achieved where the population persists. However, the condition is not necessary for the existence of disease equilibria. If the condition is violated, the function $F(\tau_p)$ is not necessarily monotone, but this does not preclude the possibility of one or more positive roots. Hence, multiple endemic equilibria or other bifurcation phenomena may occur depending on the parameters. □

Author Contributions M. Maji, L. Pujo-Menjouet and S. Khajanchi wrote the main manuscript text and M. Maji prepared figures. All authors reviewed the manuscript.

Funding This study of Mitali Maji is supported by University Grants Commission (UGC) [NTA Ref.: 211610045129], Govt. of India. Subhas Khajanchi acknowledges the financial support from the Department of Science and Technology (DST), Govt. of India, under the Scheme "Fund for Improvement of S&T Infrastructure (FIST)" [File No. SR/FST/MS-I/2019/41].

Data Availability All the used data are included in the manuscript.

Declarations

Conflict of Interest The authors declares that they have no conflict of interest.

Informed Consent Not applicable.

References

Alasmari F, Alshammari MA, Alasmari AF, Alanazi WA, Alhazzani K (2018) Neuroinflammatory cytokines induce amyloid beta neurotoxicity through modulating amyloid precursor protein levels/metabolism. Biomed Res Int 2018(1):3087475

Al-Ghraiybah NF, Wang J, Alkhalifa AE, Roberts AB, Raj R, Yang E, Kaddoumi A (2022) Glial cell-mediated neuroinflammation in Alzheimer's disease. Int J Mol Sci 23(18):10572

Banerjee S, Khajanchi S, Chaudhuri S (2015) A mathematical model to elucidate brain tumor abrogation by immunotherapy with T11 target structure. PLoS One 10(5):e0123611

Bertsch M, Franchi B, Tesi MC, Tora V (2023) The role of Aβ and Tau proteins in Alzheimer's disease: A mathematical model on graphs. J Math Biol 87(3):49

Chamberland E, Moravveji S, Doyon N, Duchesne S (2024) A computational model of Alzheimer's disease at the nano, micro, and macroscales. Front Neuroinform 18:1348113

Chen GF, Xu TH, Yan Y, Zhou YR, Jiang Y, Melcher K, Xu HE (2017) Amyloid beta: structure, biology and structure-based therapeutic development. Acta Pharmacol Sin 38(9):1205–1235

Chen CY, Tseng YH, Ward JP (2019) A mathematical model demonstrating the role of interstitial fluid flow on the clearance and accumulation of amyloid β in the brain. Math Biosci 317:108258

Chen CY, Tseng YH, Ward JP (2024) A mathematical model on the propagation of tau pathology in neurodegenerative diseases. J Math Biol 89(1):4

Ciuperca I, Pujo-Menjouet L, Matar-Tine L, Torres N, Volpert V (2024) A qualitative analysis of a Aβ-monomer model with inflammation processes for Alzheimer's disease. R Soc Open Sci 11:231536

Craft DL, Wein LM, Selkoe DJ (2002) A mathematical model of the impact of novel treatments on the Aβ burden in the Alzheimer's brain. CSF Plasma Bull Math Biol 64(5):1011–1031
De Felice FG, Wu D, Lambert MP, Fernandez SJ, Velasco PT, Lacor PN, Bigio EH, Jerecic J, Acton PJ, Shughrue PJ, Chen-Dodson E (2008) Alzheimer's disease-type neuronal tau hyperphosphorylation induced by Aβoligomers. Neurobiol Aging 29(9):1334–1347
Dear AJ, Michaels TC, Meisl G, Klenerman D, Wu S, Perrett S, Linse S, Dobson CM, Knowles TP (2020) Kinetic diversity of amyloid oligomers. Proc Natl Acad Sci U S A 117(22):12087–12094
Dear AJ, Meisl G, Aric A, Michaels TC, Kjaergaard M, Linse S, Knowles TP (2020) Identification of on- and off-pathway oligomers in amyloid fibril formation. Chem Sci 11(24):6236–6247
Dear AJ, Thacker D, Wennmalm S, Ortigosa-Pascual L, Andrzejewska EA, Meisl G, Linse S, Knowles TP (2024) Aβoligomer dissociation is catalyzed by fibril surfaces. ACS Chem Neurosci 15(11):2296–2307
DesignBuilder Software Ltd (2024) Uncertainty and sensitivity analysis. https://designbuilder.co.uk/helpv7.0/Content/UASA.htm
Doens D, Fernandez PL (2014) Microglia receptors and their implications in the response to amyloid $\beta$for Alzheimer's disease pathogenesis. J Neuroinflammation 11:1–14
Fuger P, Hefendehl JK, Veeraraghavalu K, Wendeln AC, Schlosser C, Obermuller U, Wegenast-Braun BM, Neher JJ, Martus P, Kohsaka S, Thunemann M (2017) Microglia turnover with aging and in an Alzheimer's model via long-term in vivo single-cell imaging. Nat Neurosci 20(10):1371–1376
Goure WF, Krafft GA, Jerecic J, Hefti F (2014) Targeting the proper amyloid-beta neuronal toxins: a path forward for Alzheimer's disease immunotherapeutics. Alzheimers Res Ther 6:1–15
Hamby DM (1995) A comparison of sensitivity analysis techniques. Health Phys 68(2):195–204
Hao W, Friedman A (2016) Mathematical model on Alzheimer's disease. BMC Syst Biol 10(1):1–18
Hastie T, Tibshirani R, Friedman J (2017) The elements of statistical learning: data mining, inference, and prediction, 2nd edn. Springer, New York
Hier DB, Azizi S, Thimgan MS, Wunsch DC (2022) Tau kinetics in Alzheimer's disease. Front Aging Neurosci 14:1055170
Huang YR, Liu RT (2020) The toxicity and polymorphism of β-amyloid oligomers. Int J Mol Sci 21(12):4477
Iooss B, Lemaitre P (2015) A review on global sensitivity analysis methods. Uncertainty management in simulation-optimization of complex systems: algorithms and applications. Springer, New York
Keller D, Ero C, Markram H (2018) Cell densities in the mouse brain: a systematic review. Front Neuroanat 12:83
Khajanchi S (2021) The impact of immunotherapy on a glioma immune interaction model. Chaos Solit Fractals 152:111346
Khajanchi S, Banerjee S (2017) Quantifying the role of immunotherapeutic drug T11 target structure in progression of malignant gliomas: mathematical modeling and dynamical perspective. Math Biosci 289:69–77
Lai X, Hao W, Friedman A (2020) TNF-αinhibitor reduces drug-resistance to anti-PD-1: a mathematical model. PLoS ONE 15(4):e0231499
Lindstrom MR, Chavez MB, Gross-Sable EA, Hayden EY, Teplow DB (2021) From reaction kinetics to dementia: a simple dimer model of Alzheimer's disease etiology. PLoS Comput Biol 17(7):e1009114
Magni P, Ruscica M, Dozio E, Rizzi E, Beretta G, Facino RM (2012) Parthenolide inhibits the LPS-induced secretion of IL-6 and TNF-α and NF-κB nuclear translocation in BV-2 microglia. Phytother Res 26(9):1405–1409
Maji M, Khajanchi S (2024) A fractional-order yeast prion mathematical model and its solution. J Appl Math Comput 70(4):2767–2784
Maji M, Khajanchi S (2024) Roles of astrocytes and prions in Alzheimer's disease: insights from mathematical modeling. J Biol Phys 50(2):149–179
Maji M, Khajanchi S (2025) Mathematical models on Alzheimer's disease and its treatment: a review. Phys Life Rev 52:207–244
Marino S, Hogue IB, Ray CJ, Kirschner DE (2008) A methodology for performing global uncertainty and sensitivity analysis in systems biology. J Theor Biol 254(1):178–196
McKay MD, Beckman RJ, Conover WJ (2000) A comparison of three methods for selecting values of input variables in the analysis of output from a computer code. Technometrics 42(1):55–61
Meraz-Rios MA, Toral-Rios D, Franco-Bocanegra D, Villeda-Hernandez J, Campos-Pena V (2013) Inflammatory process in Alzheimer's disease. Front Integr Neurosci 7:59
Miao J, Ma H, Yang Y, Liao Y, Lin C, Zheng J, Yu M, Lan J (2023) Microglia in Alzheimer's disease: pathogenesis, mechanisms, and therapeutic potentials. Front Aging Neurosci 15:1201982

Morimoto K, Nakajima K (2019) Role of the immune system in the development of the central nervous system. Front Neurosci 13:916
Nagaraja S, Chen L, Di Pietro LA, Reifman J, Mitrophanov AY (2019) Predictive approach identifies molecular targets and interventions to restore angiogenesis in wounds with delayed healing. Front Physiol 10:636
Ohm DT, Fought AJ, Martersteck A, Coventry C, Sridhar J, Gefen T, Weintraub S, Bigio E, Mesulam MM, Rogalski E, Geula C (2021) Accumulation of neurofibrillary tangles and activated microglia is associated with lower neuron densities in the aphasic variant of Alzheimer's disease. Brain Pathol 31(1):189–204
Pal S, Melnik R (2022) Nonlocal models in the analysis of brain neurodegenerative protein dynamics with application to Alzheimer's disease. Sci Rep 12(1):7328
Portet S, Arino J (2008) An in vivo intermediate filament assembly model. Math Biosci Eng 6(1):117–134
Puri IK, Li L (2010) Mathematical modeling for the pathogenesis of Alzheimer's disease. PLoS One 5(12):e15176
Rankin CA, Sun Q, Gamblin TC (2007) Tau phosphorylation by GSK-3βpromotes tangle-like filament morphology. Mol Neurodegener 2:1–4
Salvadores N, Moreno-Gonzalez I, Gamez N, Quiroz G, Vegas-Gomez L, Escandon M, Jimenez S, Vitorica J, Gutierrez A, Soto C, Court FA (2022) Aβoligomers trigger necroptosis-mediated neurodegeneration via microglia activation in Alzheimer's disease. Acta Neuropathol Commun 10(1):31
Sandberg A, Berenjeno-Correa E, Rodriguez RC, Axenhus M, Weiss SS, Batenburg K, Hoozemans JJ, Tjernberg LO, Scheper W (2022) Aβ42 oligomer-specific antibody ALZ-201 reduces the neurotoxicity of Alzheimer's disease brain extracts. Alzheimers Res Ther 14(1):196
Savatorova V (2023) Exploring parameter sensitivity analysis in mathematical modeling with ordinary differential equations. CODEE J 16(1):4
Simo R, Barbosa-Desongles A, Lecube A, Hernandez C, Selva DM (2012) Potential role of tumor necrosis factor-β in down regulating sex hormone-binding globulin. Diabetes 61(2):372–382
Song Y (2022) Positive invariance condition for continuous dynamical systems based on Nagumo theorem. arXiv
Song C, Zhang T, Zhang Y (2022) Conformational essentials responsible for neurotoxicity of Aβ42 aggregates revealed by antibodies against oligomeric Aβ42. Molecules 27(19):6751
Taylor R (1990) Interpretation of the correlation coefficient: a basic review. J Diagn Med Sonogr 6(1):35–39
Thompson TB, Chaggar P, Kuhl E, Goriely A, ADNI (2020) Protein-protein interactions in neurodegenerative diseases: a conspiracy theory. PLoS Comput Biol 16(10):e1008267
Tian W (2013) A review of sensitivity analysis methods in building energy analysis. Renew Sustain Energy Rev 20:411–419
Tonnies E, Trushina E (2017) Oxidative stress, synaptic dysfunction, and Alzheimer's disease. J Alzheimers Dis 57(4):1105–1121
Townsend D, Fullwood NJ, Yates EA, Middleton DA (2020) Aggregation kinetics and filament structure of a tau fragment are influenced by the sulfation pattern of the cofactor heparin. Biochemistry 59(41):4003–4014
Vidal-Itriago A, Radford RA, Aramideh JA, Maurel C, Scherer NM, Don EK, Lee A, Chung RS, Graeber MB, Morsch M (2022) Microglia morphophysiological diversity and its implications for the CNS. Front Immunol 13:997786
World Health Organization (2024) The top 10 causes of death. Available via World Health Organization website: https://www.who.int/news-room/fact-sheets/detail/the-top-10-causes-of-death
Zhang H, Wei W, Zhao M, Ma L, Jiang X, Pei H, Cao Y, Li H (2021) Interaction between A$\beta$and tau in the pathogenesis of Alzheimer's disease. Int J Biol Sci 17(9):2181
Zhang G, Wang Z, Hu H, Zhao M, Sun L (2021) Microglia in Alzheimer's disease: a target for therapeutic intervention. Front Cell Neurosci 15:749587
Zi Z (2011) Sensitivity analysis approaches applied to systems biology models. IET Syst Biol 5(6):336–346